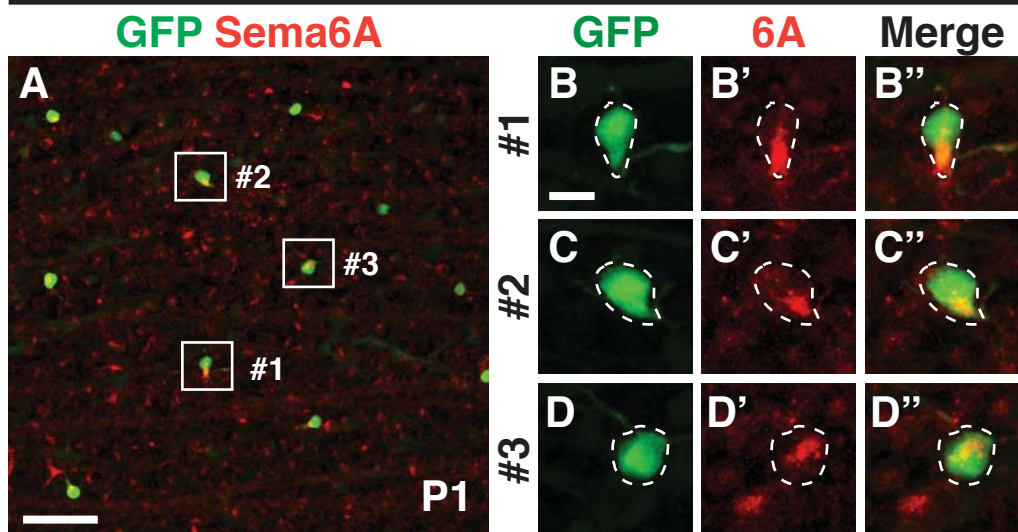
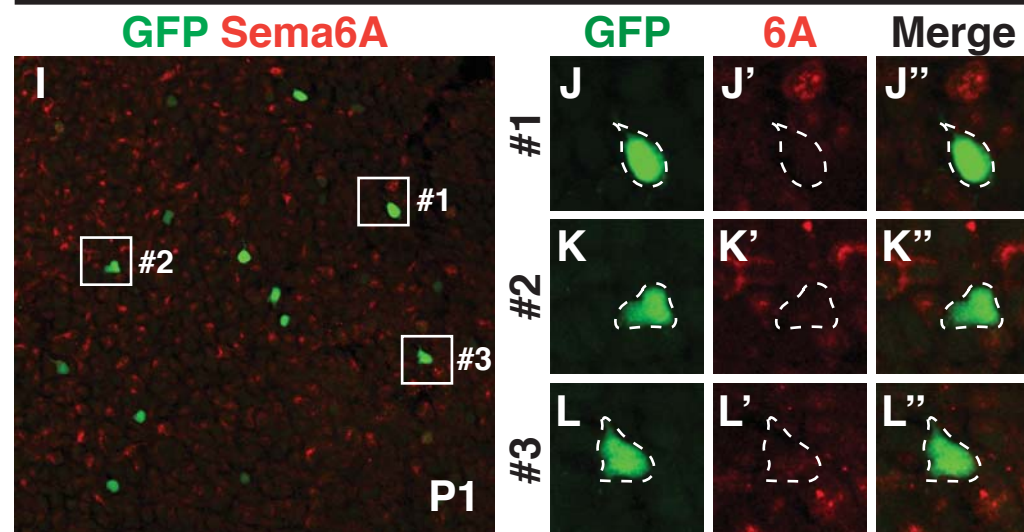
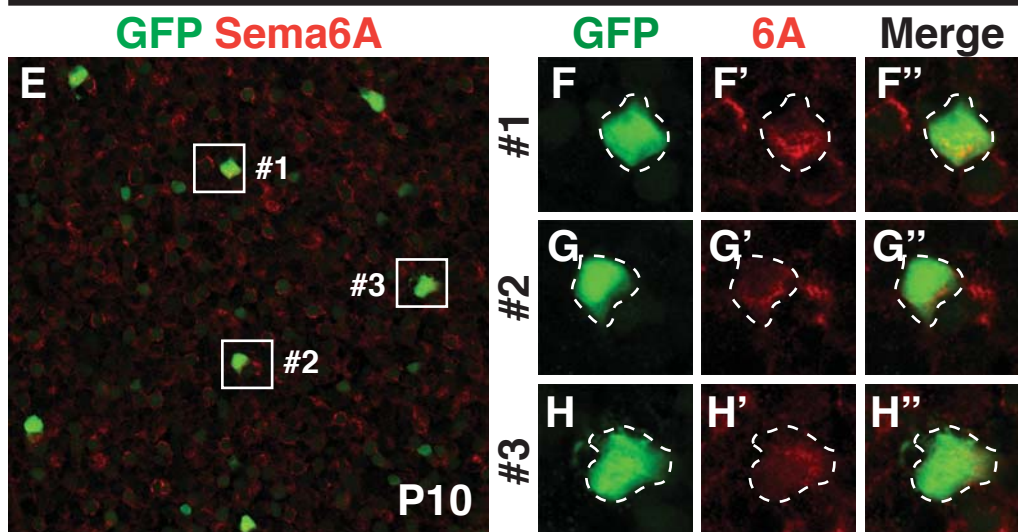
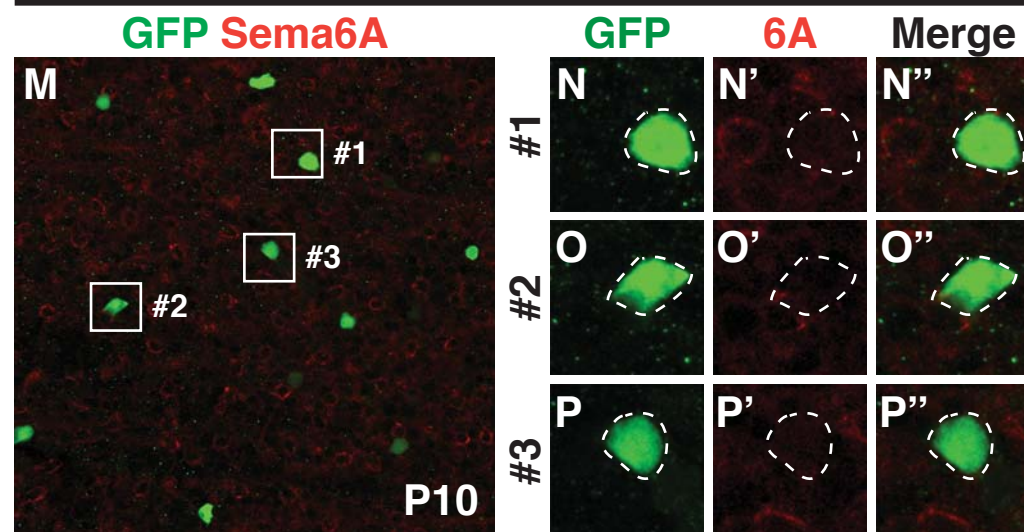
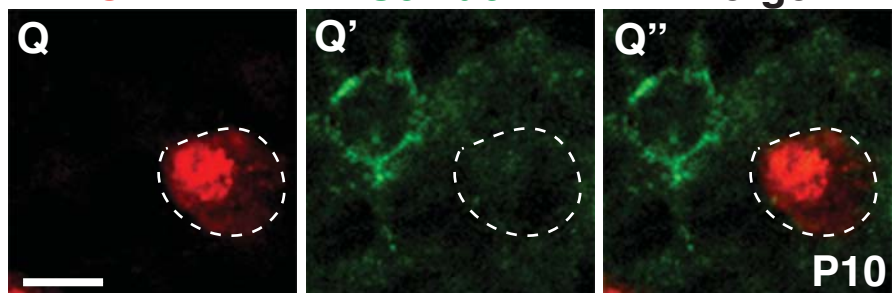
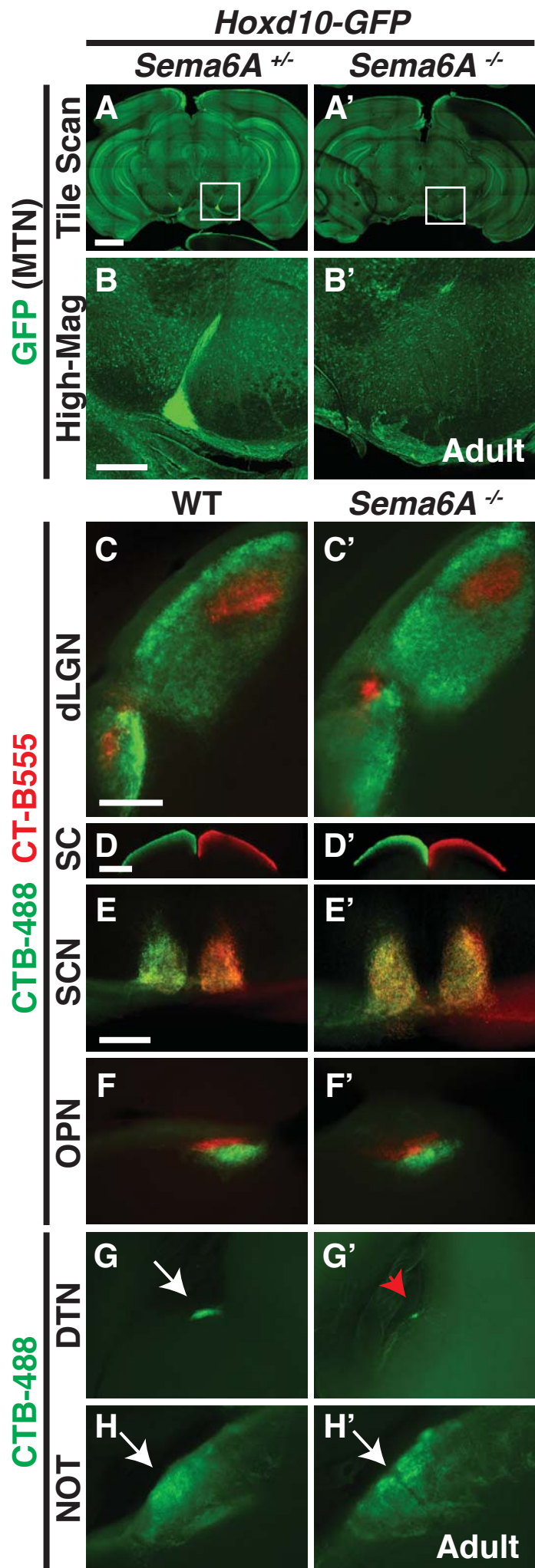


***SPIG1::GFP******DRD4-GFP******SPIG1::GFP******TRHR-GFP*****CART****Sema6A****Merge**

**Figure S1, Related to Figure 1. Characterization of Sema6A Expression in On and On-Off DSGCs During Retinal Development**

(A-D'') Wholemout immunolabeling of Sema6A in the ventral region of the P1 *SPIG1::GFP* retina (A), showing that all *SPIG1::GFP*<sup>+</sup> cells (B, C and D) express Sema6A (B', B'', C', C'', D', and D''). (E-H'') Wholemout immunostaining for Sema6A in the ventral region of the P10 *SPIG1::GFP* retina (E), showing that all *SPIG1::GFP*<sup>+</sup> cells (F, G and H) continue to express Sema6A (F', F'', G', G'', H', and H''); also see quantification in Figure 1I). (I-P'') Wholemout immunolabeling of Sema6A in P1 *DRD4-GFP* (I-L'') and P10 *TRHR-GFP* retinas (M-P''). *DRD4-GFP*<sup>+</sup> cells (J, K and L) and *TRHR-GFP*<sup>+</sup> cells (N, O and P) do not express Sema6A (J'-L'' and N'-P''); also see quantification in Figure 1I). (Q-Q'') Double immunostaining for CART (red in Q) and Sema6A (green in Q') in P10 flatmounted mouse retinas, showing that Sema6A is not expressed in CART immuno-positive cells (Q''). Scale bars: 50  $\mu$ m in (A) for (A), (E), (I), and (M); 10  $\mu$ m in (B) for (B)-(D''), (F)-(H''), (J)-(L''), and (N)-(P''); and 10  $\mu$ m in (Q) for (Q)-(Q'').



**Non-image Forming**      **Image Forming**

**AOS**

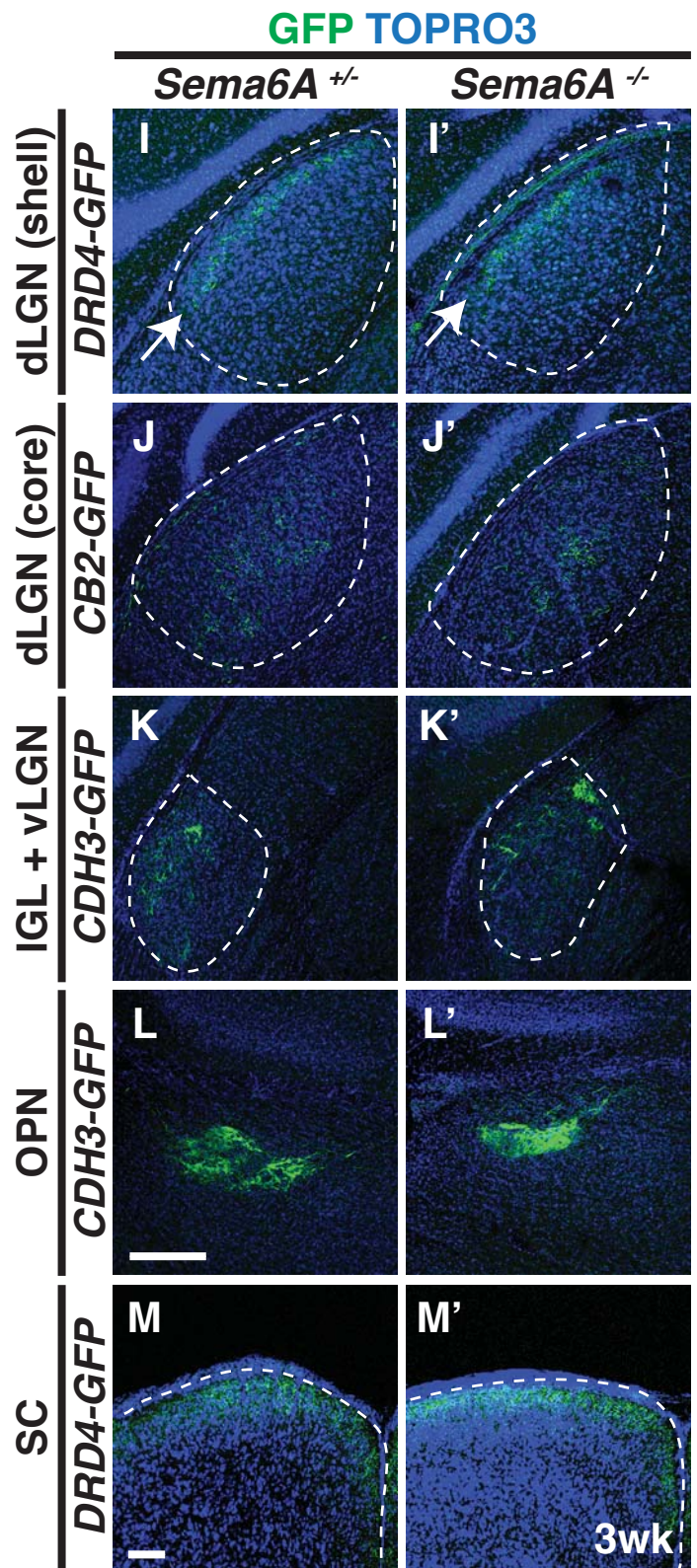


Figure S2

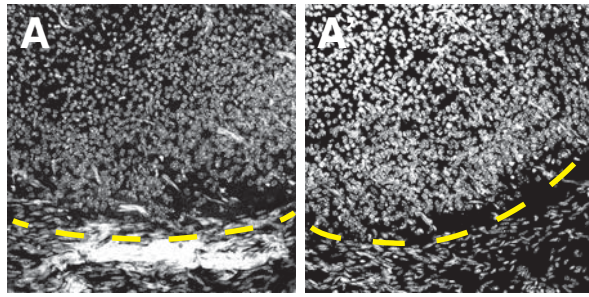
**Figure S2, Related to Figure 2. Characterization of RGC Retinorecipient Innervation in *Sema6A*<sup>-/-</sup> Mutants**

(A-B') Genetic labeling of On DSGC-MTN innervation in adult *Sema6A*<sup>+/-</sup> (A and B) and *Sema6A*<sup>-/-</sup> (A' and B') brains. *Sema6A*<sup>+/-</sup> control mice exhibit normal axonal projections to the MTN (A and B), whereas *Sema6A*<sup>-/-</sup> mutants show greatly diminished innervation (A' and B'), similar to the defects revealed by ocular CTB injections (Figure 2B'). (B) and (B') are high magnification photomicrographs of the white boxes in (A) and (A'), respectively (n=6 *Hoxd10-GFP*; *Sema6A*<sup>+/-</sup> mice; n=4 *Hoxd10-GFP*; *Sema6A*<sup>-/-</sup> mice). (C-H') Characterization of retinorecipient targeting in adult wild-type and *Sema6A*<sup>-/-</sup> mutants using ocular CTB injections. Overall RGC innervation of the image forming (dLGN in C and C', and SC in D and D') and non-image forming (SCN in E and E', and OPN in F and F') targets of the main optic visual system are preserved in *Sema6A*<sup>-/-</sup> mutants. However, *Sema6A*<sup>-/-</sup> mutants exhibit reduced innervation of the DTN (red arrowhead in G') but apparently normal innervation of the NOT (white arrow in H') in comparison to controls (white arrows in G and H) (n=4 wild-type, and n=10 *Sema6A*<sup>-/-</sup> mutants). (I-M') Characterization of retinorecipient targeting of the dLGN (I-J'), IGL and vLGN (K and K'), OPN (L and L'), and SC (M and M') using a variety of transgenic markers in *Sema6A*<sup>+/-</sup> (I-M) and *Sema6A*<sup>-/-</sup> (I'-M') mice. Overall retinorecipient innervation of multiple retinorecipient targets (dLGN, IGL and vLGN, OPN, and SC) by the indicated genetically labeled RGCs is preserved in *Sema6A*<sup>-/-</sup> mutants (n≥3 animals for each genotype characterized). Scale bars: 1mm in (A) for (A) and (A'); 100 μm in (B) for (B) and (B'); 250 μm in (C) for (C) and (C'); 250 μm in (D) for (D) and (D'); 250 μm in (E) for (E)-(H'); 250 μm in (L) for (I)-(L'); and 250 μm in (M) for (M) and (M').

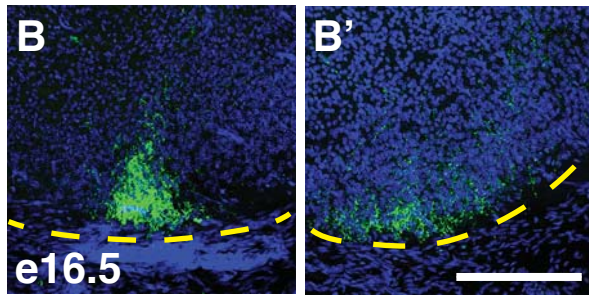
**SPIG1::GFP (MTN)**

*Sema6A*<sup>+/-</sup>      *Sema6A*<sup>-/-</sup>

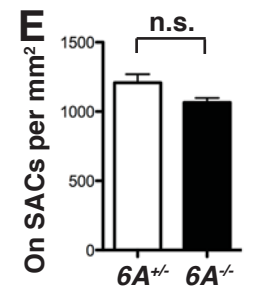
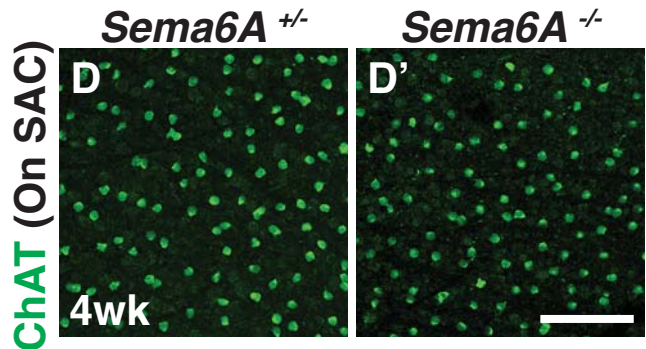
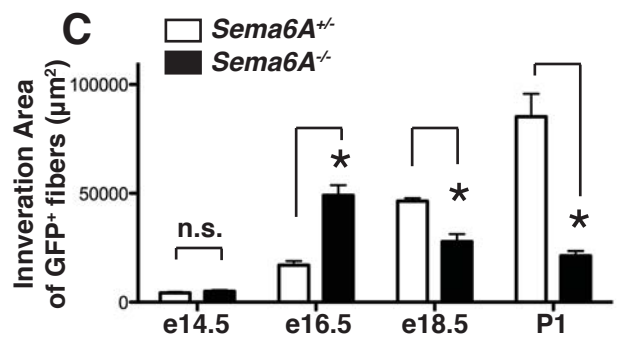
TORPO3



GFP TORPO3



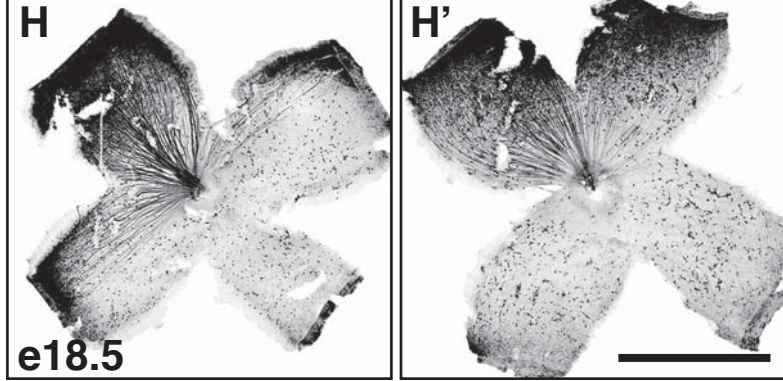
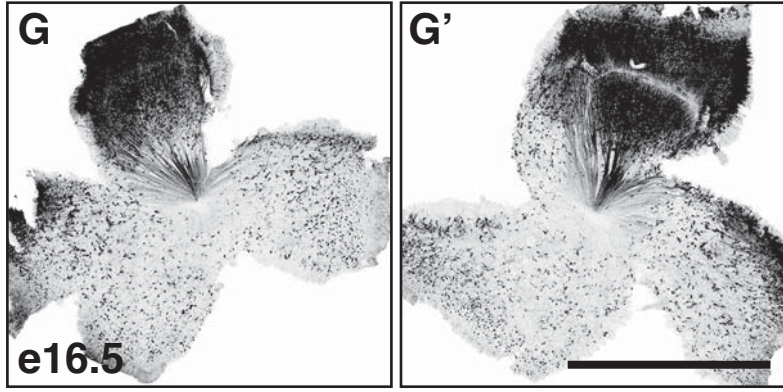
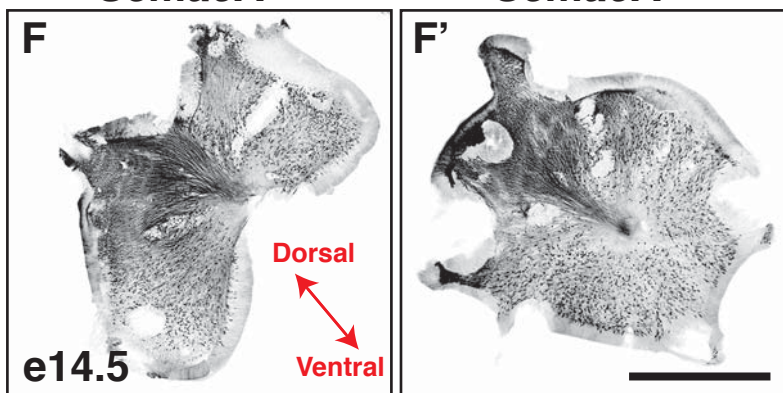
**C**



**SPIG1::GFP (retina)**

*Sema6A*<sup>+/-</sup>

*Sema6A*<sup>-/-</sup>



**SPIG1::GFP (retina)**

*Sema6A*<sup>+/-</sup>

*Sema6A*<sup>-/-</sup>

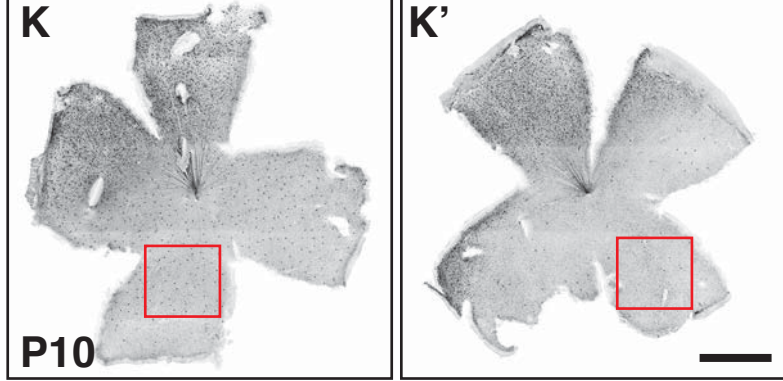
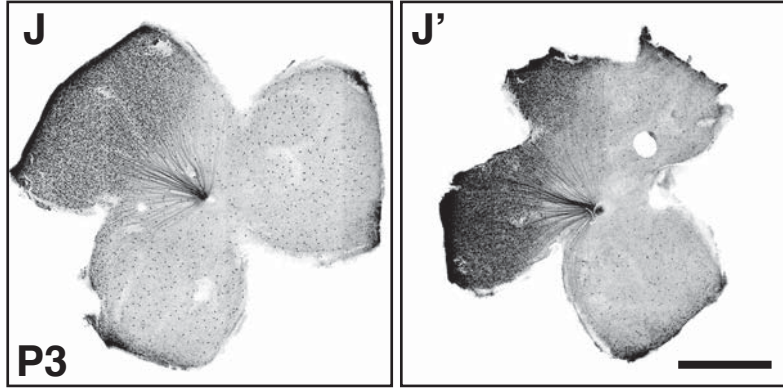
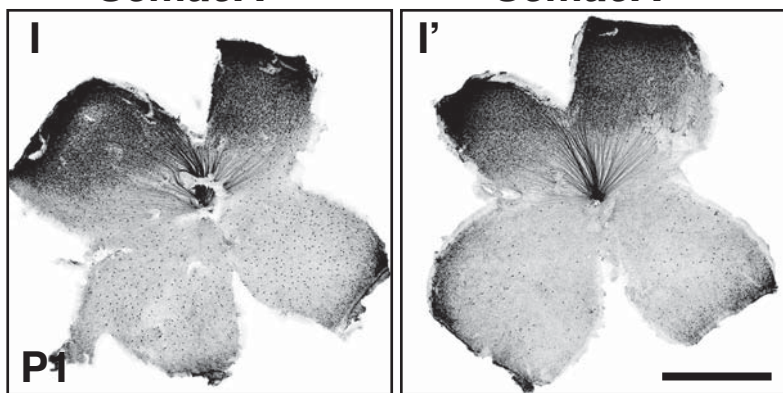


**Figure S3**

**Figure S3, Related to Figure 3. Developmental Characterization of On DSGCs in the *Sema6A*<sup>-/-</sup> Retina and On DSGC-MTN Innervation in *Sema6A*<sup>-/-</sup> Mutants**

(A-B') Characterization of the MTN target region (revealed by TORPO3 staining in A and A') and analyses of *SPIG1::GFP*<sup>+</sup> fiber projections (B and B') at e16.5 in controls (A and B) and *Sema6A*<sup>-/-</sup> mutants (A' and B'), showing that the MTN target region is apparently still intact in *Sema6A*<sup>-/-</sup> mutants at this developmental stage (compare A and A') though *SPIG1::GFP*<sup>+</sup> fibers are defasciculated (B'). (C) Quantification of *SPIG1::GFP*<sup>+</sup> fiber innervation area in controls and *Sema6A*<sup>-/-</sup> mutants (n≥3 animals for each time point and for both genotypes analyzed). \**P*<0.001. (D and D') Representative *en face* images of On SACs in 4 week-old *Sema6A*<sup>+/-</sup> (D) and *Sema6A*<sup>-/-</sup> (D') retinas. (E) Quantification of On SAC density in *Sema6A*<sup>+/-</sup> and *Sema6A*<sup>-/-</sup> retinas (n=5 control and *Sema6A*<sup>-/-</sup> retinas, *P*=0.07184). (F-K') Tile-scanned images of flat-mounted *SPIG1::GFP*; *Sema6A*<sup>+/-</sup> (F-K) and *SPIG1::GFP*; *Sema6A*<sup>-/-</sup> retinas (F'-K') from e14.5 to P10. No difference is observed between controls and *Sema6A*<sup>-/-</sup> mutants at e14.5 (F and F'), e16.5 (G and G'), and e18.5 (H and H') (see the quantification in Figure 3J). However, the number of *SPIG1::GFP*<sup>+</sup> cells in the ventral region of *Sema6A*<sup>-/-</sup> retinas exhibits a significant decrease at P1 (compare I and I'), and this defect persists throughout postnatal retinal development (compare J and J', K and K'). The red boxes in (K) and (K') represent regions where quantification was conducted in Figure 3J. Error bars represent SEM. Scale bars: 200 μm in (B') for (A)-(B'); 100 μm in (D') for (D) and (D'); 1 mm in (F') for (F) and (F'); 1 mm in (G') for (G) and (G'); 1 mm in (H') for (H) and (H'); 1 mm in (I') for (I) and (I'); 1 mm in (J') for (J) and (J'); and 1 mm in (K') for (K) and (K').

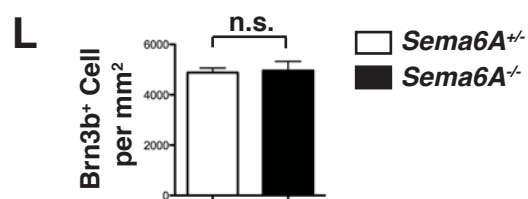
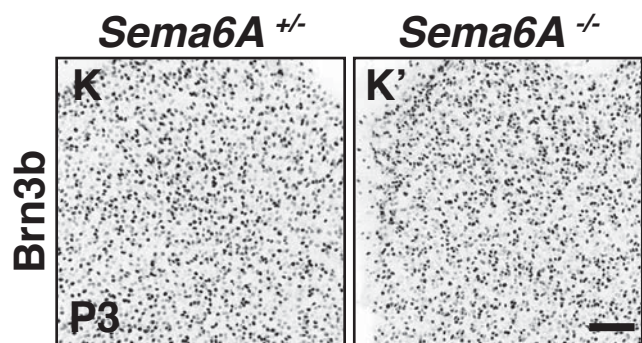
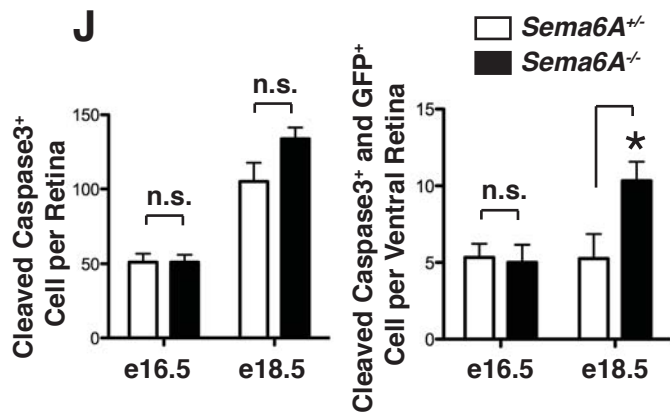
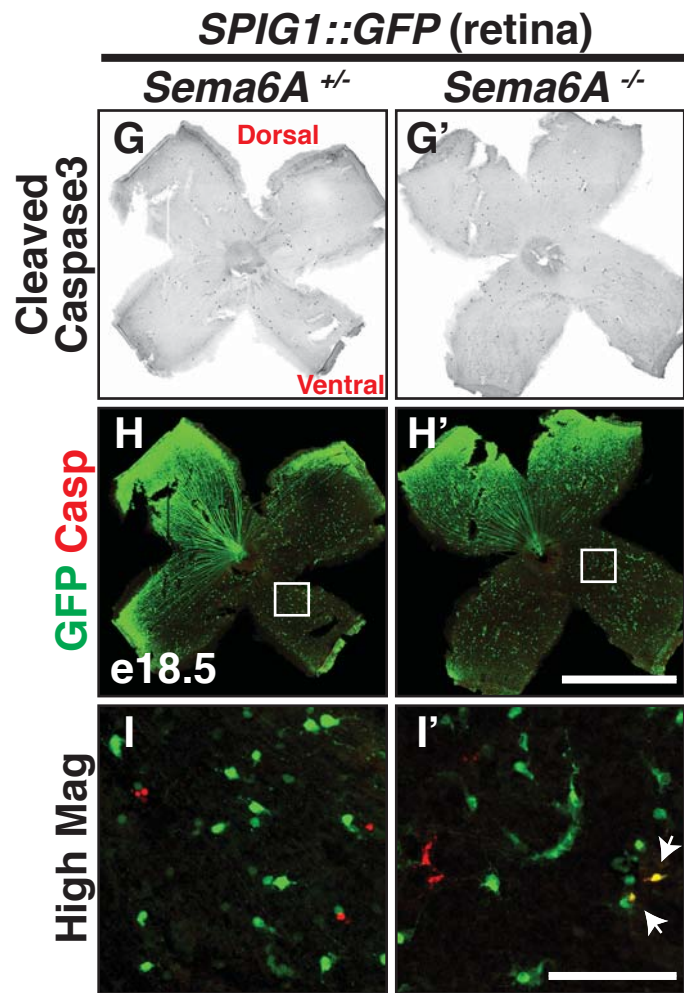
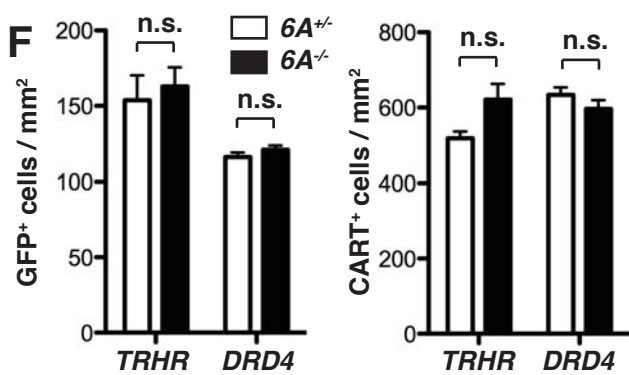
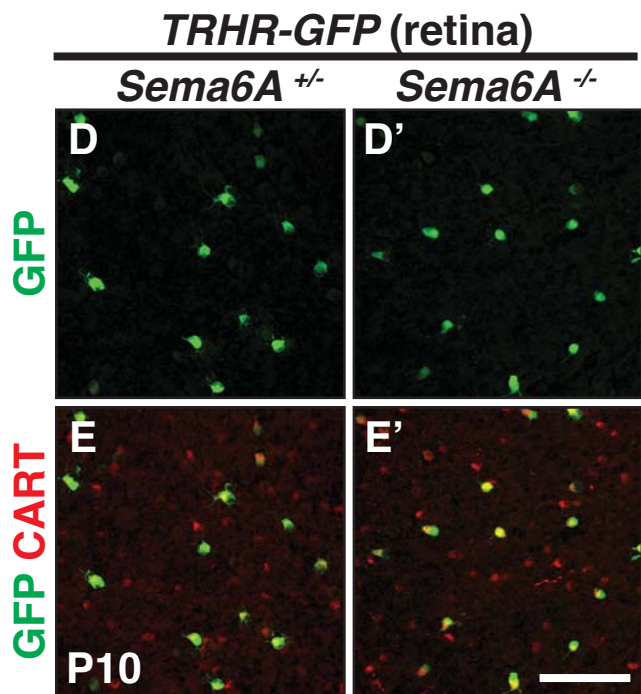
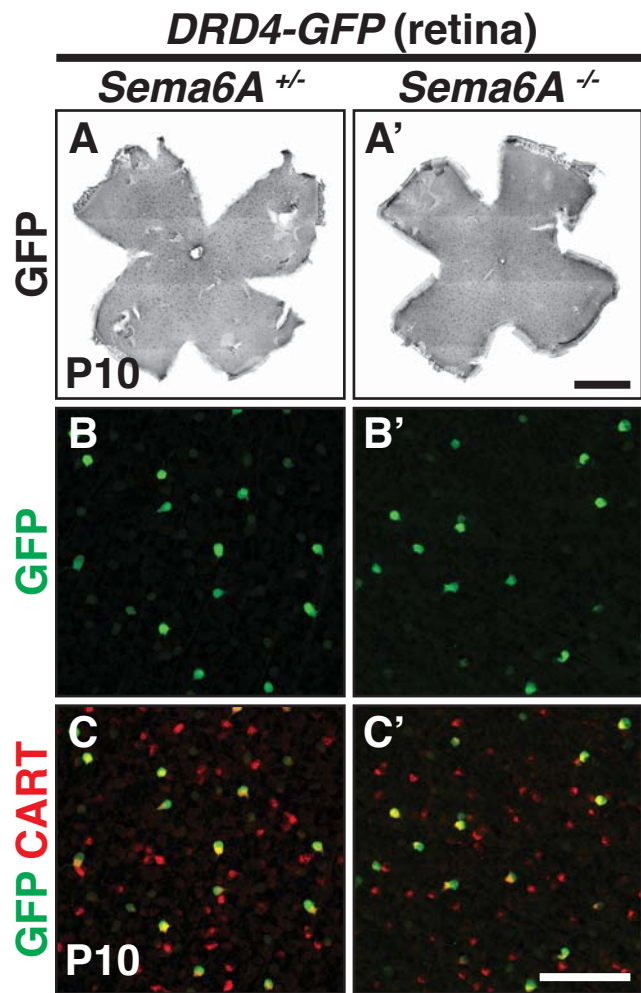


Figure S4

**Figure S4, Related to Figure 3. *Sema6A*<sup>-/-</sup> Mutants Exhibit the Normal Number of On-Off DSGC but Enhanced Cell Apoptosis in On DSGCs**

(A and A') Representative, tile-scanned, images of a P10 *DRD4-GFP*; *Sema6A*<sup>+/-</sup> retina (A) and a P10 *DRD4-GFP*; *Sema6A*<sup>-/-</sup> retina (A') immunostained with an antibody directed against GFP. No difference was found between control and *Sema6A*<sup>-/-</sup> retinas with respect to *DRD4-GFP*<sup>+</sup> cell number (see quantification in Figure S4F). (B-C') Double immunostaining of P10 *DRD4-GFP*; *Sema6A*<sup>+/-</sup> (B and C) and *DRD4-GFP*; *Sema6A*<sup>-/-</sup> retinas (B' and C') with antibodies against GFP (green in B and B') and CART (red in C and C'). No difference was observed between controls and *Sema6A*<sup>-/-</sup> mutants with respect to *DRD4-GFP*<sup>+</sup> or *CART*<sup>+</sup> cell number (see quantification in Figure S4F). (D-E') Immuno-labeling of *TRHR-GFP*<sup>+</sup> On-Off DSGCs (D and D') and *CART*<sup>+</sup> On-Off DSGCs (E and E') in P10 *Sema6A*<sup>+/-</sup> (D and E) and *Sema6A*<sup>-/-</sup> (D' and E') retinas. (F) Quantification of *TRHR-GFP*<sup>+</sup>, *DRD4-GFP*<sup>+</sup>, and *CART*<sup>+</sup> On-Off DSGCs in control and *Sema6A*<sup>-/-</sup> retinas at P10 (n=6 *DRD4-GFP*; *Sema6A*<sup>+/-</sup> retinas; n=6 *DRD4-GFP*; *Sema6A*<sup>-/-</sup> retinas; n=4 *TRHR-GFP*; *Sema6A*<sup>+/-</sup> retinas; and n=4 *TRHR-GFP*; *Sema6A*<sup>-/-</sup> retinas). (G-I') Double immunolabeling of e18.5 *SPIG1::GFP*; *Sema6A*<sup>+/-</sup> (G-I) and *SPIG1::GFP*; *Sema6A*<sup>-/-</sup> retinas (G'-I') with antibodies against cleaved Caspase-3 (a marker for cells undergoing cell apoptosis, G and G') and GFP (merged in H and H'). (I) and (I') are high-magnification images of the white box regions in (H) and (H'), respectively. (J) Left panel shows quantification for total cleaved Caspase-3<sup>+</sup> cell number per retina in control and *Sema6A*<sup>-/-</sup> mutants; right panel shows the quantification of cleaved Caspase-3<sup>+</sup> and *SPIG1::GFP*<sup>+</sup> double immuno-positive cells in the ventral region of *Sema6A*<sup>+/-</sup> and *Sema6A*<sup>-/-</sup> retinas (n=3 retinas for control and *Sema6A*<sup>-/-</sup> mutants at e16.5; n=4 retinas for control at e18.5; and n=6 retinas for *Sema6A*<sup>-/-</sup> mutants at e18.5). \**P*=0.03398. (K and K') Representative images of flatmounted *Sema6A*<sup>+/-</sup> and *Sema6A*<sup>-/-</sup> P3

retinas immunostained with anti-Brn3b. **(L)** Quantification of Brn3b<sup>+</sup> RGCs in P3 *Sema6A*<sup>+/-</sup> and *Sema6A*<sup>-/-</sup> retinas (n=4 retinas for both genotypes, *P*=0.8550). Error bars represent SEM. Scale bars: 1 mm in (A') for (A) and (A'); 100 μm in (C') for (B)-(C'); 100 μm in (E') for (D)-(E'); 1 mm in (H') for (G)-(H'); 100 μm in (I') for (I) and (I'); and 100 μm in (K') for (K) and (K').

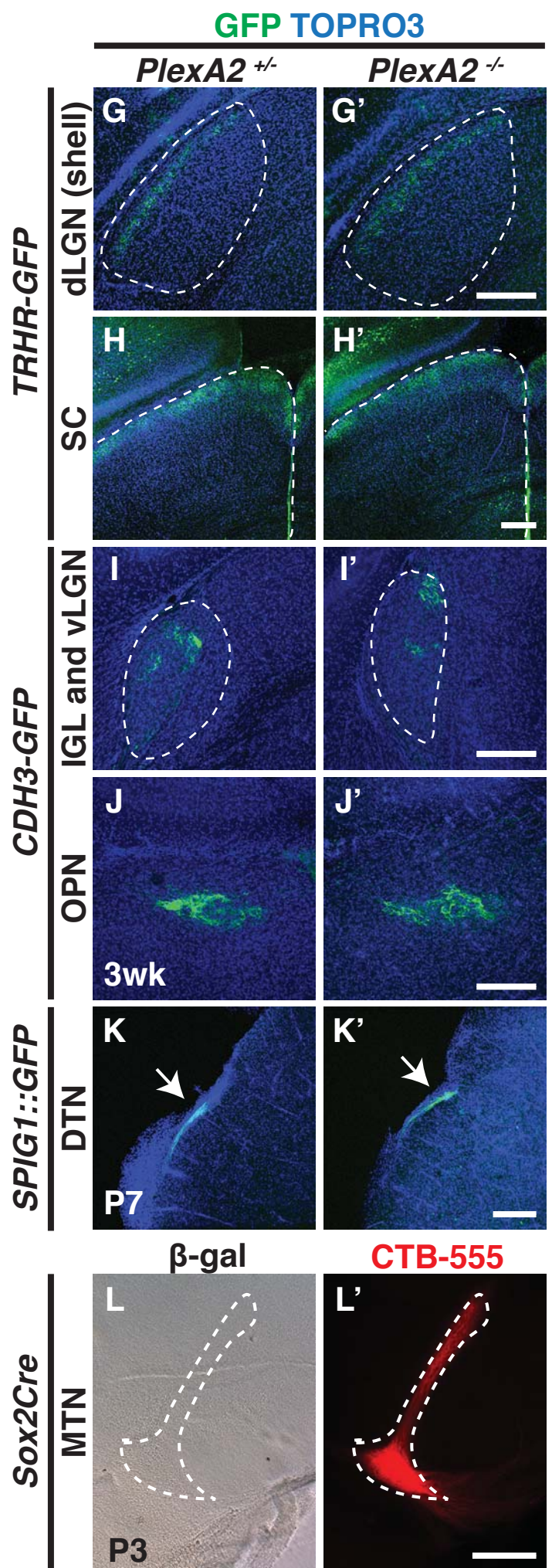
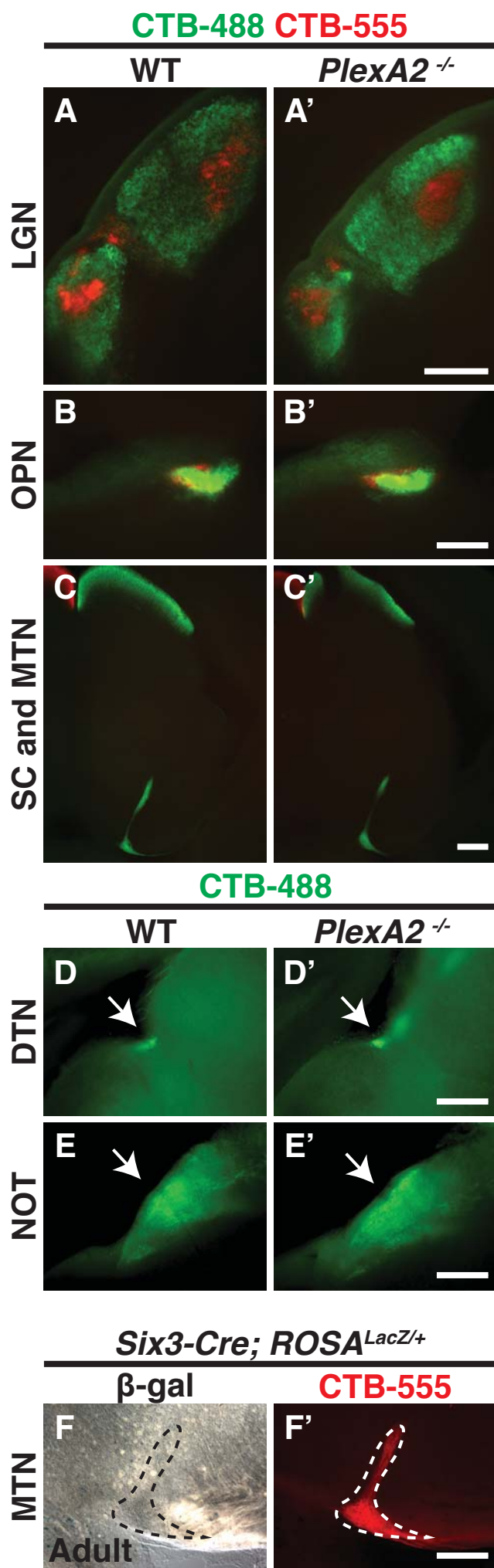


Figure S5

**Figure S5, Related to Figure 4. *PlexA2*<sup>-/-</sup> Mutants Show Normal Retinorecipient Innervation of Main and Accessory Optic System Central Targets**

(A-E') Characterization of retinorecipient targeting in WT (A-E) and *PlexA2*<sup>-/-</sup> mutants (A'-E') following ocular CTB injections. Compared to WT animals, *PlexA2*<sup>-/-</sup> mice exhibit normal targeting to the LGN (A'), OPN (B'), SC and MTN (C'), DTN (D'), and NOT (E') (n=4 WT; n=8 *PlexA2*<sup>-/-</sup> mutants). (F and F') Ocular CTB injection and subsequent LacZ staining in sections of adult *Six3-Cre; ROSA<sup>LacZ/+</sup>* midbrain, showing that Six3-Cre is not expressed in the MTN (n=2 animals). (G-K') Detailed characterization of genetically labeled RGC axon projections to the dLGN (G and G'), SC (H and H'), IGL and vLGN (I and I'), OPN (J and J'), and DTN (K and K') in *PlexA2*<sup>+/-</sup> (G-K) and *PlexA2*<sup>-/-</sup> (G'-K') mice. *PlexA2*<sup>-/-</sup> mutants exhibit normal retinorecipient targeting for all GC subtypes examined (n≥3 animals for each genotype characterized). (L and L') LacZ staining in sections of P3 *Sox2Cre* midbrain, a control showing that the MTN region is LacZ<sup>-</sup> (n=2 animals). Scale bars: 250 μm.

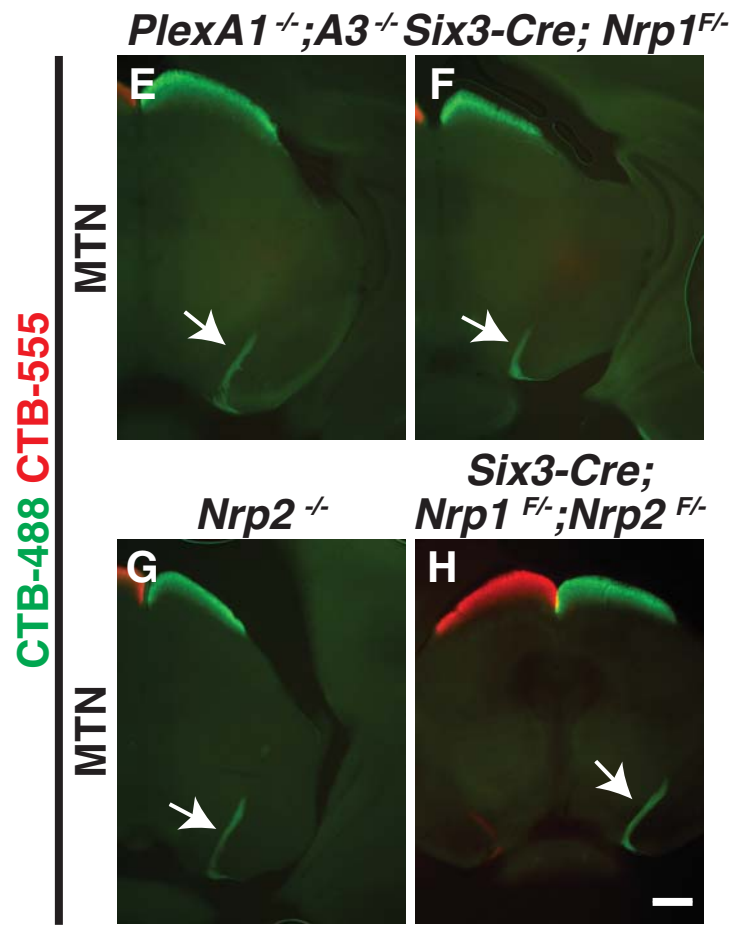
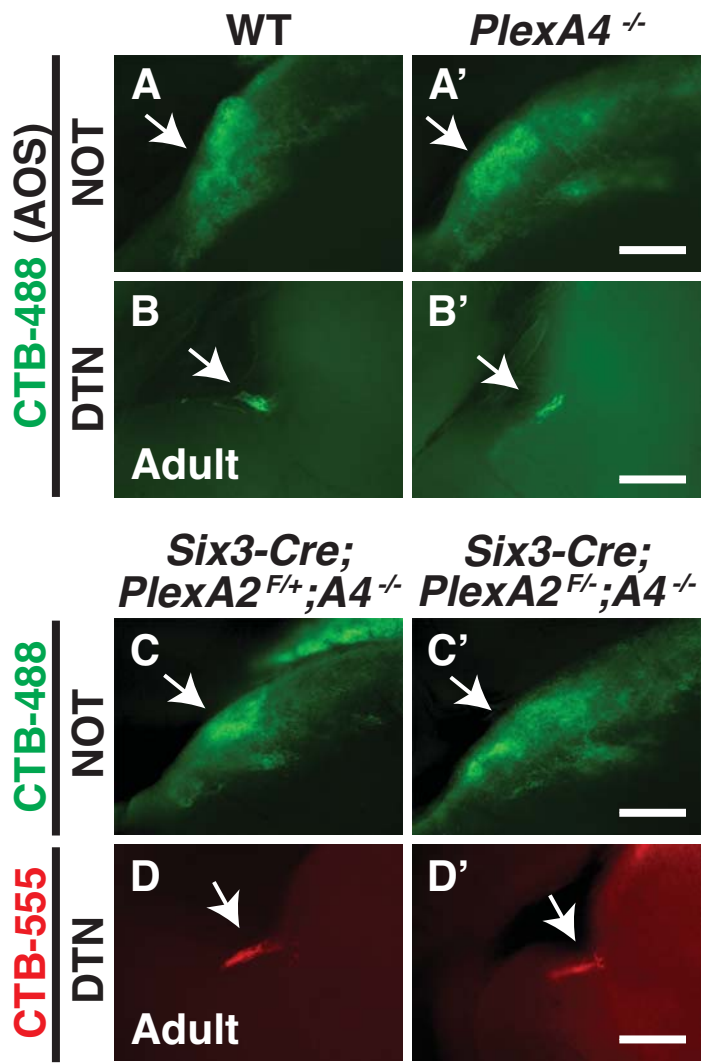


Figure S6

**Figure S6, Related to Figure 5. Analyses of Accessory Optic System Development in Multiple *PlexA* and *Nrp* Mutants.**

(A-B') *PlexA4*<sup>-/-</sup> mutants (A' and B') exhibit normal AOS retinorecipient targeting to the NOT (A') and DTN (B') compared to WT animals (A and B) (n=4 WT; n=5 *PlexA4*<sup>-/-</sup> mutants). (C-D') Characterization of AOS retinorecipient targeting in *Six3-Cre;PlexA2*<sup>F/+</sup>;*PlexA4*<sup>-/-</sup> (C and D) and *Six3-Cre;PlexA2*<sup>F/-</sup>;*PlexA4*<sup>-/-</sup> mice (C' and D'). Note that the AOS targeting to the NOT and to the DTN is preserved in *Six3-Cre;PlexA2*<sup>F/-</sup>;*PlexA4*<sup>-/-</sup> mice as compared to the control (n=4 animals for both genotypes). (E-H) RGC-MTN projections appear normal in *PlexA1*<sup>-/-</sup>;*PlexA3*<sup>-/-</sup> (E), *Six3Cre;Nrp1*<sup>F/-</sup> (F), *Nrp2*<sup>-/-</sup> (G), and *Six3Cre;Nrp1*<sup>F/-</sup>;*Nrp2*<sup>F/-</sup> mutant mice (H) (n=3 animals for each genotype). Scale bars: 250 μm.

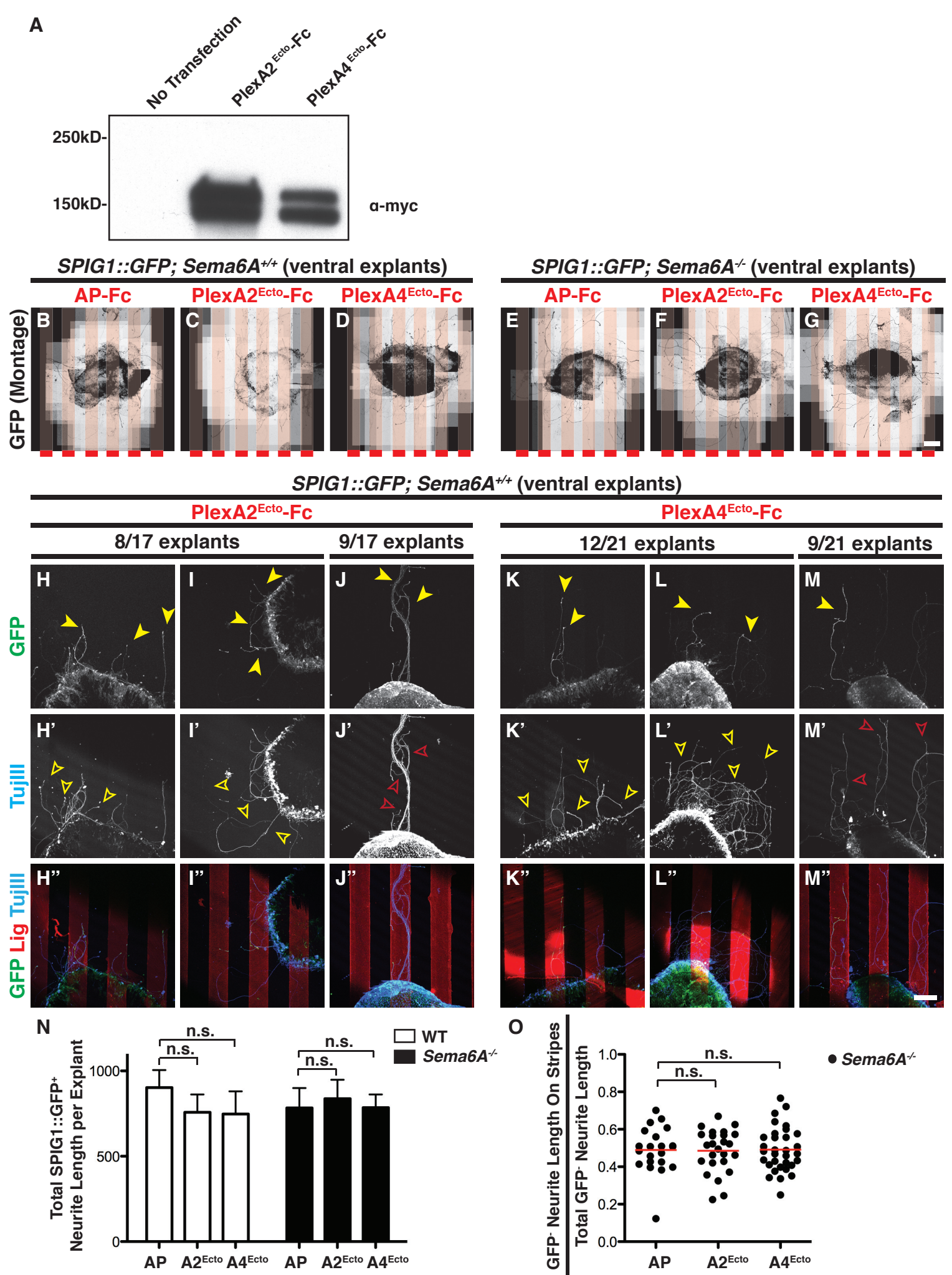


Figure S7

**Figure S7, Related to Figure 6. Biochemical Characterization of PlexA2/A4 Ectodomain Recombinant Proteins and Neurite Stripe Assay.**

(A) Biochemical characterization of PlexA2<sup>Ecto</sup> and PlexA4<sup>Ecto</sup> recombinant proteins from the concentrated supernatants obtained from transfected 293T cells that secrete these recombinant proteins (see Supplemental Experimental Procedures for details). PlexA2<sup>Ecto</sup> and PlexA4<sup>Ecto</sup> recombinant proteins are Myc-tagged and are detected in this Western blot using a monoclonal antibody raised against the Myc epitope. (B-G) Montage images of multiple *SPIG1::GFP*; *Sema6A*<sup>+/+</sup> ventral retina explants (B-D) and *SPIG1::GFP*; *Sema6A*<sup>-/-</sup> ventral retina explants (E-G) on AP-Fc (B and E), PlexA2<sup>Ecto</sup>-Fc (C and F), and PlexA4<sup>Ecto</sup>-Fc stripes (D and G). The light red transparent bars in each panel cover the stripes coated with different ligands. n=19 (B), 17 (C), 21 (D), 21 (E), 24 (F), and 35 (G) explants. (H-M'') Representative images showing that GFP<sup>+</sup> neurites from *SPIG1::GFP*; *Sema6A*<sup>+/+</sup> ventral retina explants preferentially extend on PlexA2<sup>Ecto</sup> (filled yellow arrowheads in H-J) or PlexA4<sup>Ecto</sup> stripes (filled yellow arrowheads in K-M). In contrast, some GFP<sup>-</sup> TujIII<sup>+</sup> neurites in ~1/2 of the explants exhibit no growth preference on PlexA2<sup>Ecto</sup> stripes (yellow open arrowheads in H' and I'; observed in 8 out of 17 explants) or PlexA4<sup>Ecto</sup> stripes (yellow open arrowheads in K' and L'; observed in 12 out of 21 explants). In the remaining explants, all GFP<sup>-</sup> TujIII<sup>+</sup> neurites still exhibit attraction to PlexA2<sup>Ecto</sup> stripes (red open arrowheads in J'; 9 out of 17 explants) and PlexA4<sup>Ecto</sup> stripes (red open arrowheads in M'; 9 out of 21 explants). Explants in (H) and (K) are the same explants as those in Figures 6F and 6G, respectively. (N) Quantification of total *SPIG1::GFP*<sup>+</sup> neurite length (μm) per explant, showing that overall GFP<sup>+</sup> neurite growth is not statistically different among the different experimental groups. (O) Quantification of the ratio of *SPIG1::GFP*<sup>-</sup> TujIII<sup>+</sup> neurite lengths on stripes over total *SPIG1::GFP*<sup>-</sup> TujIII<sup>+</sup> neurite lengths from *Sema6A*<sup>-/-</sup> explants. Red bars represent mean

values of each group. Error bars, SEM. Scale bars: 100  $\mu\text{m}$  in (G) for (B)-(G); and 100  $\mu\text{m}$  in (M'') for (H)-(M'').

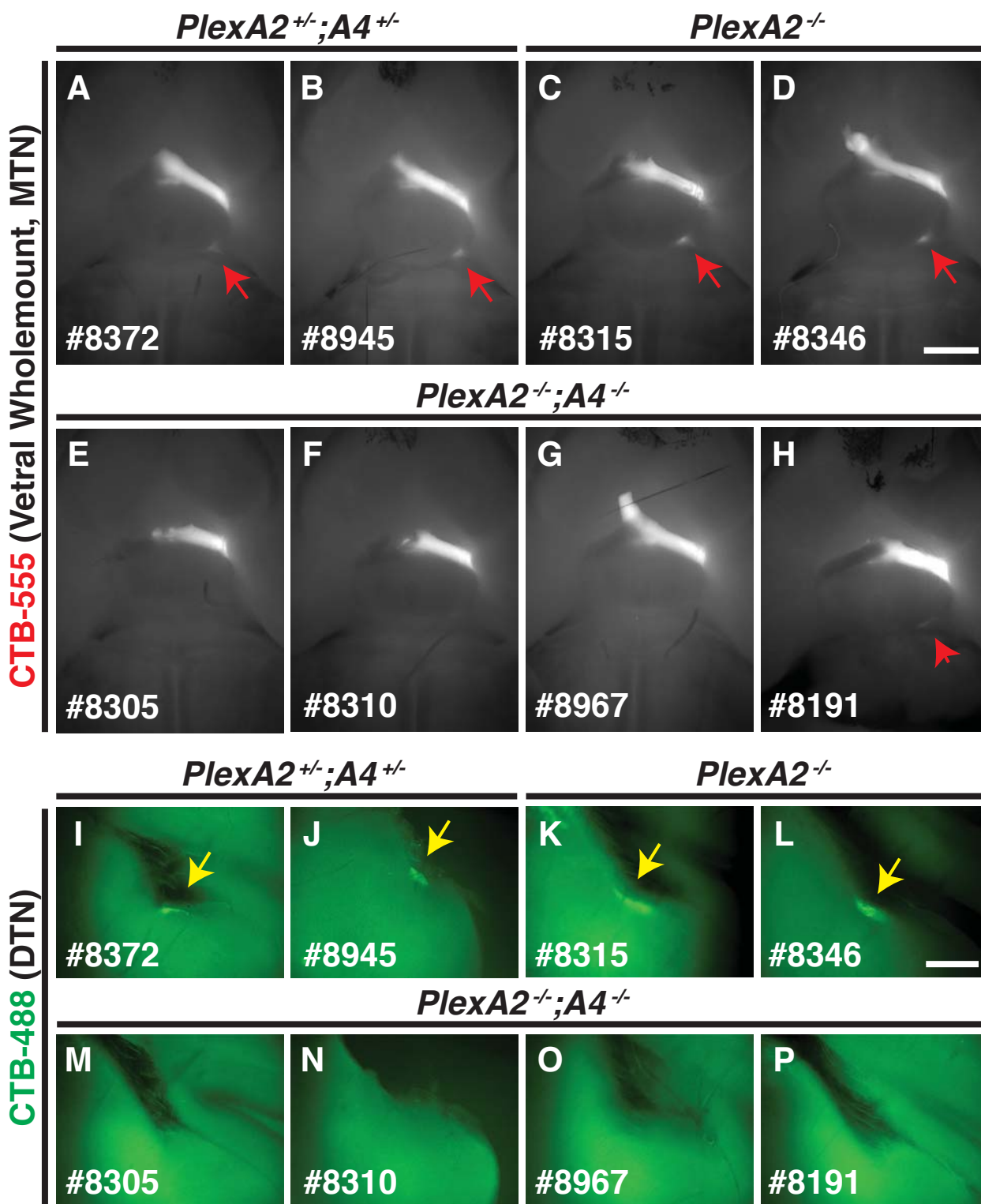


Figure S8

**Figure S8, Related to Figure 7. Post-hoc Characterization of *PlexA2*<sup>-/-</sup>;*PlexA4*<sup>-/-</sup> AOS Axon Projections**

(A-H) Wholemount ventral view of *PlexA2*<sup>+/-</sup>;*PlexA4*<sup>+/-</sup> (A and B), *PlexA2*<sup>-/-</sup> (C and D), and *PlexA2*<sup>-/-</sup>;*PlexA4*<sup>-/-</sup> (E-H) brains following ocular CTB injections. Note that all *PlexA2*<sup>+/-</sup>;*PlexA4*<sup>+/-</sup> (A and B) and *PlexA2*<sup>-/-</sup> mice (C and D) exhibit normal RGC-MTN innervation (red arrows in A, B, C, and D), whereas all *PlexA2*<sup>-/-</sup>;*PlexA4*<sup>-/-</sup> mice (E to G), except for #8191 (H, red arrowhead), show greatly diminished innervation to the MTN. The weak MTN innervation in mouse #8191 is correlated with the preserved vertical OKR in this animal (Figure 7E, black arrow). (I-P) Cross-sectional view of the DTN innervation in *PlexA2*<sup>+/-</sup>;*PlexA4*<sup>+/-</sup> (I and J), *PlexA2*<sup>-/-</sup> (K and L), and *PlexA2*<sup>-/-</sup>;*PlexA4*<sup>-/-</sup> (M-P). *PlexA2*<sup>+/-</sup>;*PlexA4*<sup>+/-</sup> and *PlexA2*<sup>-/-</sup> mice show normal DTN innervation (yellow arrows in I, J, K, and L), whereas all *PlexA2*<sup>-/-</sup>;*PlexA4*<sup>-/-</sup> mice exhibit no DTN innervation (M-P). Scale bars: 1 mm in (D) for (A)-(H); and 250 μm in (L) for (I)-(P).

## SUPPLEMENTAL EXPERIMENTAL PROCEDURES

### Animals

The day of vaginal plug observation was designated embryonic day 0.5 (e0.5), and the day of birth in this study was designated postnatal day 0 (P0). *Semaphorin 6A*<sup>-/-</sup> (*Sema6A*<sup>-/-</sup>), *plexin A1*<sup>-/-</sup> (*PlexA1*<sup>-/-</sup>), *plexin A2*<sup>-/-</sup> (*PlexA2*<sup>-/-</sup>), *plexin A3*<sup>-/-</sup> (*PlexA3*<sup>-/-</sup>), *plexin A4*<sup>-/-</sup> (*PlexA4*<sup>-/-</sup>), *plexin A2*<sup>f</sup> (*PlexA2*<sup>f</sup>), *neuropilin1*<sup>f</sup> (*Nrp1*<sup>f</sup>), *neuropilin 2*<sup>-/-</sup> (*Nrp2*<sup>-/-</sup>), and *Six3-Cre* mouse lines were described previously (Sun et al., 2013). The GFP knock-in line *SPIG1::GFP* and GFP BAC transgenic lines (*Hoxd10-GFP*, *TRHR-GFP*, *DRD4-GFP*, *CB2-GFP*, and *Cdh3-GFP*) were described previously (Dhande et al., 2013; Huberman et al., 2008; Huberman et al., 2009; Kay et al., 2011; Osterhout et al., 2011; Rivlin-Etzion et al., 2011; Yonehara et al., 2009; Yonehara et al., 2008). The *Sox2-Cre* mouse line (stock number: 004783) and *ROSA*<sup>LacZ/+</sup> reporter mouse line (stock number: 003309) were obtained from the Jackson Laboratory.

### Immunohistochemistry

Primary antibodies used in this study include: goat-anti-mouse Sema6A (R&D systems, 1:200), rabbit anti-GFP (Lifescience Technologies, IgG fraction, 1:1000), rabbit anti-GFP (Lifescience Technologies, serum, 1:1000), chicken anti-GFP (AVES, 1:1000), rabbit anti-CART (Phoenix Pharmaceuticals Inc., 1:1000), goat anti-ChAT (Millipore, 1:200), TO-PRO3 (Lifescience Technologies, 1:500), rabbit anti-cleaved Caspase 3(Asp 175) (5A1E) (Cell Signaling Technology, 1:200), rabbit anti-Brn3b (gift from Dr. Jeremy Nathans, 1:200), rabbit anti-plexinA2 (gift from Dr. Fumikazu Suto, 1:200), Armenian hamster anti-plexinA4 (gift from Dr. Fumikazu Suto, 1:200), and mouse anti-TujIII (Promega, 1:1000).

### **Wholemout Retina Staining**

Wholemout retina ICC was performed as previously described (Sun et al., 2013). Briefly, enucleated eyeballs were fixed in 4% paraformaldehyde (PFA) for 1 hour at 4°C. The eyecups were dissected out and incubated for 4-5 days at room temperature with primary antibodies in PBS containing 5% donkey serum, 0.1% Triton X-100 and 20% dimethyl sulphoxide (DMSO). Retinas were washed with PBS+0.1% Triton X-100 5 times for 1 hour at room temperature and then incubated with secondary antibodies in PBS+ 0.1% Triton X-100+ 2% donkey serum overnight at 4°C. Retinas were washed in PBS+0.1% Triton X-100 5 times for 1 hour at room temperature and then flat mounted. Confocal images were taken using a Zeiss LSM 700 confocal microscope.

### **Cholera Toxin Subunit B (CTB) Injection**

Bilateral CTB injection was performed as previously described (Riccomagno et al., 2014). Briefly, the adult animals were anesthetized using isophorone and then injected with 2  $\mu$ L CTB-Alexa-555 or CTB-Alexa-488 (Life Technologies, 1mg/mL) bilaterally into the vitreous of each eye. For neonatal pups, the animals were placed on ice for anesthesia and then injected with 1  $\mu$ L CTB-Alexa solutions bilaterally. One to two days after the procedure, the animals were perfused with 4% PFA; the brains were then dissected out and further sectioned using Leica VT1000 S Fully Automatic Vibrating Blade Microtome.

### **Alkaline Phosphatase (AP) Staining**

AP staining was performed as previously described (Sun et al., 2013) with minor modifications. Animals were perfused with 4% PFA and brains were dissected out and post-fixed in 4% PFA

for 2 hours in 4°C. The brains were rinsed 3 times for 10 minutes with PBS and then sectioned (250 µm) using a Leica VT1000 S Fully Automatic Vibrating Blade Microtome. The brain slices were rinsed twice in HBSS at room temperature and then incubated in a 65°C water bath for 2 hours to inactivate endogenous alkaline phosphatases. After heat inactivation, the brain slices were rinsed 3 times for 10 min at room temperature with B1 buffer containing 0.1 M Tris (pH7.5) and 0.15 M NaCl. The tissues were then rinsed 3 times for 10 min with B3 buffer containing 0.1 M Tris (pH9.5) and 0.1 M NaCl, 50 mM MgCl<sub>2</sub> and 5 mM levamisole. AP activity was then visualized by incubation with 37.5 g/mL NBT (Roche), 175 g/mL BCIP (Roche) in B3 buffer at room temperature until the AP-generated precipitate appeared.

### **X-gal Staining**

X-gal staining was performed as previously described (Matsuoka et al., 2011). Brain slices (250 µm) were sectioned with a vibrotome and rinsed twice in PBS before the staining. Brain slices were then stained with 5mM potassium ferricyanide, 5mM potassium ferrocyanide, 2mM MgCl<sub>2</sub> and 1 mg/ml X-gal for 1–2 h at room temperature. Tissue sections were rinsed in PBS and bright-field images were taken.

### **Tissue Clearance Using Benzyl Alcohol and Benzyl Benzoate (BABB)**

Brain slices (after AP staining or X-gal staining) were dehydrated using methanol-H<sub>2</sub>O solution and cleared using BABB solution. Briefly, brain slices were dehydrated sequentially in 25%, 50%, 75%, 95%, and 100% methanol at room temperature (20 minutes per dilution). The tissues were then rinsed in 50% methanol / 50% BABB solution (BABB: 1 part Benzyl Alcohol and 2 parts of benzyl Benzoate) for 1 hour at room temperature and then transferred into 100% BABB

solution until they were clear (10-20 minutes for the brain slices). The tissues were mounted in BABB solution on slides for imaging.

### **Measurement and Quantification of SPIG1::GFP<sup>+</sup> Fiber Innervation Area and Intensity**

The innervation area of SPIG1::GFP<sup>+</sup> fibers was measured using the ImageJ “Freehand Selections” tool. The MTN innervation areas in 2-to-3 adjacent sections from 1 animal were measured and the mean innervation area value was determined for statistical analysis. For the measurement and quantification of SPIG1::GFP<sup>+</sup> fiber intensity, the innervation area was first selected by the “Freehand Selections” tool. Within the innervation region, the “Integrated Intensity” of the GFP fluorescent signals was determined using the ImageJ “Measurement” tool, providing a readout of the sum of all SPIG1::GFP<sup>+</sup> fiber intensities in the selected innervation region. The mean value of integrated intensity for each animal was determined by the measurement of 2-to-3 adjacent midbrain sections.

### **Generation and concentration of PlexA2<sup>Ecto</sup>-Fc and PlexA4<sup>Ecto</sup>-Fc recombinant proteins**

pcDNA3.0-PlexA2<sup>Ecto</sup>-Fc expression plasmid (amino acids 35-1232 of mouse plexin A2) was kindly provided by Dr. Roman Giger. The ectodomain of mouse plexin A4 (amino acids 24-1229) was subcloned into the same vector. PlexA2<sup>Ecto</sup>-Fc and PlexA4<sup>Ecto</sup>-Fc plasmids were introduced into HEK293T cells by Lipofectamine 2000 (Life Technologies) and the conditioned medium were harvested 72hrs later. The recombinant proteins were concentrated by Amicon® Ultra 15 mL Filters (Millipore, 100K NMWL), and protein concentrations were further determined by NanoDrop 8000 spectrophotometer (Thermo Scientific).

### **Fluorescent Ligand Binding Assay**

COS7 cells were plated on coverslips in 24-well plates ( $5 \times 10^4$  cells/well), transfected with mouse Sema6A expression plasmid for 48 hours and then rinsed briefly under room temperature with HBH buffer containing 0.5mg/mL BSA, 20mM HEPES (pH7.0), 5mM  $\text{CaCl}_2$ , 1mM  $\text{MgCl}_2$ , and 1X HBSS buffer (Life Technologies). Ligands (AP-Fc, PlexA2<sup>Ecto</sup>-Fc, and PlexA4<sup>Ecto</sup>-Fc; 10nM) were pre-clustered in HBH buffer with goat anti-Human Fc antibody (Cy3 conjugated) (Sigma C2571; 2 $\mu\text{g}/\text{ml}$ ) for 1 hour at 4 degree, and then were added to COS7 cells that had been rinsed with HBH buffer. The cells were incubated with ligands for 1 and  $\frac{1}{4}$  hours at room temperature with gentle shaking before being rinsed 6 times for 10 minutes with HBH buffer. The COS7 cells were then fixed 30 seconds with acetone/formaldehyde fixative (60% acetone, 1.1% formaldehyde, 20mM HEPES (pH7.0)). COS7 cells were further rinsed 3 times for 10 minutes before imaging with a Zeiss 700 confocal microscope.

### **Stripe Assay**

The axon guidance stripe assay was performed as previously described (Sun et al., 2013). Briefly, ligands (AP-Fc, PlexA2<sup>Ecto</sup>-Fc, and PlexA4<sup>Ecto</sup>-Fc; 50  $\mu\text{g}/\text{ml}$ ) were pre-clustered with goat anti-Human IgG (Fc specific) (Sigma; 2 $\mu\text{g}/\text{mL}$ ) in 1X HBSS buffer (Life Technologies) for 1 hour at 4 degree. Retinas obtained from e17.5 mouse embryos were dissected in cold L-15 medium (Gibco). The ventral region of SPIG1::GFP<sup>+</sup> retinas was carefully dissected out under a Zeiss fluorescent dissection scope and further cut into small explants. The explants were then transferred onto 60 mm cell culture plates (Falcon) coated with 100  $\mu\text{g}/\text{mL}$  poly-D-lysine (Sigma), 5  $\mu\text{g}/\text{mL}$  laminin (Life Technologies), and alternating stripes ( $\sim 80 \mu\text{m}$  in width) of 50  $\mu\text{g}/\text{mL}$  ligands mixed with Alexa-555-conjugated BSA (10  $\mu\text{g}/\text{mL}$ ) to allow for detection by

fluorescence illumination. The explants were allowed to grow on the plates with stripes for 2 days in neurobasal culture medium containing 50 units/mL penicillin, 50 units/mL streptomycin, B-27 supplement, 2 mM L-Glutamine, 10 ng/mL ciliary neurotrophic factor (CNTF, R&D Systems), 50 ng/mL brain-derived neurotrophic factor (BDNF, Peprotech), 5mM forskolin, and 5 µg/mL insulin. The explants were fixed in 4% PFA for 10 minutes and immunostained with antibodies directed against GFP (chick anti-GFP from Aves Lab Incorporation, 1:1000) and  $\beta$ III tubulin (mouse anti- $\beta$ III tubulin from Promega, 1:1000). GFP<sup>+</sup> neurite lengths were measured and quantified using ImageJ plugins.

### **Optokinetic Reflex (OKR) Measurement**

The OKR apparatus and recording methodology are as previously described (Cahill and Nathans, 2008). In brief, a head-posted mouse was immobilized in an acrylic holder in the center of a 29.5 cm diameter vertical white cylinder. A computer-generated image of alternating black and white vertical stripes (each stripe subtending 4 degrees of visual angle) was projected into the inner walls of the drum by a rotating projector mounted on the ceiling. The striped pattern had an average brightness of 100-200 lux and was rotated at 5°/sec. 30-second stimulus presentations were alternated with 30 seconds of a uniform grey. Eye movements were captured with an infrared video imaging system (ISCAN, Cambridge, MA), and stored, processed and displayed using Microsoft Excel. The number of eye tracking movements (ETMs; defined as a saccade followed by a slow tracking movement in the opposite direction) was counted per 30-second interval. Eye movements along the vertical axis (with respect to the mouse) were recorded by rotating the acrylic mouse holder 90 degrees so that the nose of the mouse pointed vertically. With the stripes moving dorsal-to-ventral or ventral-to-dorsal with respect to the

mouse, the same rotating visual stimulus was presented only to the eye from which the infrared video recording was obtained. The OKR testing and data analyses were performed without knowledge of mouse genotypes.

### **Statistical Analysis**

Statistical significance of differences between mean values among two or more groups was determined using Student's t test or one-way ANOVA analysis followed by Tukey's HSD test, respectively. The criterion for statistical significance was set at  $P < 0.05$ .

## SUPPLEMENTAL REFERENCES

Cahill, H., and Nathans, J. (2008). The optokinetic reflex as a tool for quantitative analyses of nervous system function in mice: application to genetic and drug-induced variation. *PloS one* *3*, e2055.

Dhande, O.S., Estevez, M.E., Quattrochi, L.E., El-Danaf, R.N., Nguyen, P.L., Berson, D.M., and Huberman, A.D. (2013). Genetic dissection of retinal inputs to brainstem nuclei controlling image stabilization. *The Journal of neuroscience : the official journal of the Society for Neuroscience* *33*, 17797-17813.

Huberman, A.D., Manu, M., Koch, S.M., Susman, M.W., Lutz, A.B., Ullian, E.M., Baccus, S.A., and Barres, B.A. (2008). Architecture and activity-mediated refinement of axonal projections from a mosaic of genetically identified retinal ganglion cells. *Neuron* *59*, 425-438.

Huberman, A.D., Wei, W., Elstrott, J., Stafford, B.K., Feller, M.B., and Barres, B.A. (2009). Genetic identification of an On-Off direction-selective retinal ganglion cell subtype reveals a layer-specific subcortical map of posterior motion. *Neuron* *62*, 327-334.

Kay, J.N., De la Huerta, I., Kim, I.J., Zhang, Y., Yamagata, M., Chu, M.W., Meister, M., and Sanes, J.R. (2011). Retinal ganglion cells with distinct directional preferences differ in molecular identity, structure, and central projections. *The Journal of neuroscience : the official journal of the Society for Neuroscience* *31*, 7753-7762.

Matsuoka, R.L., Chivatakarn, O., Badea, T.C., Samuels, I.S., Cahill, H., Katayama, K., Kumar, S.R., Suto, F., Chedotal, A., Peachey, N.S., *et al.* (2011). Class 5 transmembrane semaphorins control selective Mammalian retinal lamination and function. *Neuron* *71*, 460-473.

Osterhout, J.A., Josten, N., Yamada, J., Pan, F., Wu, S.W., Nguyen, P.L., Panagiotakos, G., Inoue, Y.U., Egusa, S.F., Volgyi, B., *et al.* (2011). Cadherin-6 mediates axon-target matching in a non-image-forming visual circuit. *Neuron* *71*, 632-639.

Riccomagno, M.M., Sun, L.O., Brady, C.M., Alexandropoulos, K., Seo, S., Kurokawa, M., and Kolodkin, A.L. (2014). Cas adaptor proteins organize the retinal ganglion cell layer downstream of integrin signaling. *Neuron* *81*, 779-786.

Rivlin-Etzion, M., Zhou, K., Wei, W., Elstrott, J., Nguyen, P.L., Barres, B.A., Huberman, A.D., and Feller, M.B. (2011). Transgenic mice reveal unexpected diversity of on-off direction-selective retinal ganglion cell subtypes and brain structures involved in motion processing. *The Journal of neuroscience : the official journal of the Society for Neuroscience* *31*, 8760-8769.

Sun, L.O., Jiang, Z., Rivlin-Etzion, M., Hand, R., Brady, C.M., Matsuoka, R.L., Yau, K.W., Feller, M.B., and Kolodkin, A.L. (2013). On and off retinal circuit assembly by divergent molecular mechanisms. *Science* *342*, 1241974.

Yonehara, K., Ishikane, H., Sakuta, H., Shintani, T., Nakamura-Yonehara, K., Kamiji, N.L., Usui, S., and Noda, M. (2009). Identification of retinal ganglion cells and their projections involved in central transmission of information about upward and downward image motion. *PloS one* 4, e4320.

Yonehara, K., Shintani, T., Suzuki, R., Sakuta, H., Takeuchi, Y., Nakamura-Yonehara, K., and Noda, M. (2008). Expression of SPIG1 reveals development of a retinal ganglion cell subtype projecting to the medial terminal nucleus in the mouse. *PloS one* 3, e1533.